Effects Seen in the Passage of Positively Charged Ions through Single Crystals*

R. E. Holland and D. S. Gemmell

Argonne National Laboratory, Argonne, Illinois

(Received 26 February 1968)

This paper reports on some effects seen when swift, positively charged light ions are passed through various monocrystalline materials. The main part of the work concerns blocking effects observed when protons in the energy range 3–12 MeV were passed through thin ($\sim$10 mg/cm²) monocrystals of silicon. The energies and spatial distributions of the emergent particles were recorded both with photographic plates and with an automated scanning detector. In addition to the usual distribution of particles produced by Rutherford scattering, the spatial distributions are observed to include sharp lines corresponding to the planes of the target crystal. The observed widths of these lines are found to vary inversely as the square root of the energy of the incident ion. A calculation which traced the paths of ions through a hypothetical rigid lattice gave results qualitatively in agreement with observation. Photographic plates exposed to protons from the reaction $Si^{28}(d,p)Si^{29}$ occurring in a silicon crystal showed blocking phenomena similar to those observed with elastically scattered protons. In the angular region in which scattering is changing to blocking, the intensities of particles show a behavior that could be the result of wave phenomena.

1. INTRODUCTION

THERE has been considerable interest recently in phenomena associated with the passage of positively charged ions through monocrystals. Much of the experimental work on this subject has been concerned with effects related to the "channeling" of charged particles in crystals. Channeling occurs when the incident ion beam is nearly parallel to a major plane of the crystal. Under these conditions, the ions emerging from the crystal at small angles relative to the incident beam are observed[1] to be preferentially concentrated into directions corresponding to major crystal planes. This is presumed[1-3] to result from the collective steering effect of an ordered array of atoms. Positively charged ions that find themselves traveling between major planes of atoms in a crystal and in a direction making a small angle with these planes suffer a series of correlated small scatterings as they pass successive atomic layers in the crystal. Nelson and Thompson[1] showed that the collective effect of these small deflections is to steer the ions to and fro in the space ("channel") between planes. Thus, ions that are injected at small angles to a major plane become trapped or "channeled" in the direction of the plane.

Several of the interesting phenomena observed result directly from the fact that channeled ions travel through a crystal in trajectories that do not closely approach the atomic nuclei of the crystal. Thus the rate of nuclear reaction between crystal nuclei and incident ions is greatly reduced[4-6] when channeling occurs. Furthermore, channeled particles sample mainly the low-density part of the electron cloud in the crystal and consequently their rate of energy loss is abnormally low.[7-11] Other experiments show that both the production of characteristic x rays[12] and of radiation damage[13] are strongly dependent on channeling of the incident beam. That the channeling mechanism can be understood as an oscillation of particles trapped between planes has been nicely demonstrated by experiments at Oak Ridge National Laboratory.[14]

The present paper is concerned principally with effects associated with particle trajectories that originate at lattice sites. These trajectories are distinct from those of channeled ions. We consider ions which emerge (or appear to emerge) from the nuclei of the crystal—for example, particles produced in nuclear reactions involving the crystal nuclei or positive ions observed at wide angles (i.e., outside the region of multiple scattering) in Rutherford scattering. If the incident beam has an energy of a few MeV, then most particles observed in wide-angle Rutherford scattering by a thin monocrystal will have suffered a single large-angle scattering. The impact parameter involved in such a collision is typically on the order of 10^{-12} cm. Thus, on the scale of the crystal lattice (where the distances involved are typically a few times 10^{-8} cm), the scattered particle may be assumed to originate from a crystal nucleus.

Particles originating from a nucleus in this way and in a direction close to that of a major crystal plane encounter a high density of scattering centers. Thus one

---

* Work performed under the auspices of the Atomic Energy Commission.

[1] R. S. Nelson and M. W. Thompson, Phil. Mag. 8, 1677 (1963).

[2] J. Lindhard, Phys. Letters 12, 126 (1964); Kgl. Danske Videnskab. Selskab, Mat. Fys. Medd. 34, No. 14 (1965).

[3] C. Erginsoy, Phys. Rev. Letters 15, 360 (1965).

[4] E. Bøgh, J. A. Davies, and K. O. Nielsen, Phys. Letters 12, 129 (1964).

[5] M. W. Thompson, Phys. Rev. Letters 13, 756 (1965).

[6] D. S. Gemmell and R. E. Holland, Phys. Rev. Letters 14, 945 (1965).

[7] G. Dearnaley, IEEE Trans. Nucl. Sci. 11, 249 (1964).

[8] C. Erginsoy, H. E. Wegner, and W. M. Gibson, Phys. Rev. Letters 13, 530 (1964).

[9] A. R. Sattler and G. Dearnaley, Phys. Rev. Letters 15, 59 (1965).

[10] W. M. Gibson, C. Erginsoy, H. E. Wegner, and B. R. Appleton, Phys. Rev. Letters 15, 357 (1965).

[11] S. Datz, T. S. Noggle, and C. D. Moak, Phys. Rev. Letters 15, 254 (1965).

[12] W. Brandt, J. M. Khan, D. L. Potter, R. D. Worley, and H. P. Smith, Jr., Phys. Rev. Letters 14, 42 (1965).

[13] T. S. Noggle and O. S. Oen, Phys. Rev. Letters 16, 395 (1966).

[14] H. O. Lutz, S. Datz, C. D. Moak, and T. S. Noggle, Phys. Rev. Letters 17, 285 (1966).

expects to see a minimum in the number of ions of this type emerging in directions corresponding to major crystal planes. The observation of such an effect (which we have called a "blocking" effect) was reported earlier[6] for the case of proton elastic scattering and in (d, p) reactions in various crystals. Blocking effects in elastic scattering experiments have also been reported by a group at Moscow State University[15] and a group at the University of Aarhuus[16] has used the scattered particles to study channeling. Angular dependences in the emission of α particles and conversion electrons from radioactive atoms embedded in monocrystals have also been reported.[17,18]

Figure 1 illustrates a simplified model of the blocking of a particle (charge Z_1e and energy E) emitted from a nucleus within the crystal and traveling near a direction in which there is a chain of atoms with interatomic spacing l. The nuclei of the crystal atoms have charge Z_2e. We neglect electronic screening effects, recoil effects, and possible channeling effects. If the nuclei are further assumed not to vibrate, then such a model predicts the complete extinction of particles emitted in a small cone around this direction. This extinction is entirely due to Rutherford scattering from the nearest-neighbor atom in the chain. A particle initially emitted at a small angle γ to the chain of atoms will suffer an additional angular deflection ψ introduced by the Rutherford scattering at the nearest-neighbor atom. Thus for small values of γ and ψ the total angle between the direction of travel and the chain of atoms is
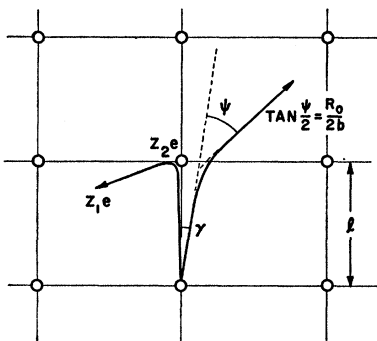
$$\gamma + \psi = b/l + R_0/b,$$

FIG. 1. Simple model illustrating positive ions emitted from a nucleus. The shadow effect is produced by Rutherford scattering at the nearest-neighbor atom.

[15] A. F. Tulinov, V. S. Kulikauskas, and M. N. Malov, Phys. Letters **18**, 304 (1965); A. F. Tulinov, Dokl. Akad. Nauk SSSR **162**, 546 (1965) [English transl.: Soviet Phys.—Doklady **10**, 463 (1965)]; A. F. Tulinov, B. G. Akhmetova, A. A. Pusunov, and A. A. Bednjakov, Zh. Eksperim. i Teor. Fiz. Pis'ma v Redaktsiyu **2**, 48 (1965) [English transl.: Soviet Phys.—JETP Letters **2**, 30 (1965)].
[16] E. Bøgh and E. Uggerhøj, Phys. Letters **17**, 116 (1965).
[17] B. Domeij and K. Björkqvist, Phys. Letters **14**, 127 (1965); B. Domeij, Arkiv Fysik **32**, 179 (1966).
[18] G. Astner, I. Bergström, B. Domeij, L. Eriksson, and Å. Persson, Phys. Letters **14**, 308 (1965).
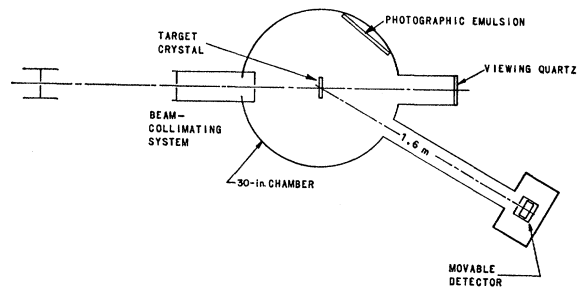

FIG. 2. Schematic diagram of experimental arrangement.

where b is the impact parameter in the Rutherford scattering and $R_0 = Z_1 Z_2 e^2/E$ is the classical distance of closest approach in a head-on collision. By minimizing this total angle with respect to the impact parameter b, one can readily show that the total angular width of the shadow region is

$$\beta = [16 Z_1 Z_2 e^2/lE]^{1/2}. \qquad (1)$$

For 4-MeV protons emitted along a major axis in a silicon crystal, Eq. (1) gives $\beta \approx 1°$. Recoil and screening effects may be expected to reduce the angular width of the anomaly. Thermal vibrations and channeling effects may also be expected to modify the value of β and to permit some transmission in the direction of the atomic chain. In this simple model the value of β is highly dependent on the direction of emission of the particle since the value of l varies rapidly with direction in the crystal.

The measurements reported previously[6] showed that the observed angular width of blocking lines is only about a sixth of the value given by Eq. (1). Furthermore, the width is seen to be independent of direction within the plane—in contradiction to the predictions of this model. In this paper, we describe the previous work in more detail and in addition report new measurements made with an improved apparatus.

2. EXPERIMENTAL PROCEDURE

All of the data were recorded with a 30-in. scattering chamber installed on one of the beam lines of the Argonne Tandem Van de Graaff accelerator. A monocrystalline target was mounted in the center of the chamber on a goniometer which allowed the crystal to be rotated about an axis perpendicular to its surface and in addition about two mutually perpendicular axes (vertical and horizontal) which were also perpendicular to the beam direction. Figure 2 shows a schematic diagram of the target chamber and the experimental setup. The thin target crystal mounted on the goniometer could be accurately oriented by observing the fluorescence pattern that the channeling of the transmitted beam produced on a piece of quartz situated at the rear of the scattering chamber. The characteristic patterns associated with major axes of the target crystal

were easily recognized on the quartz viewer. This procedure enabled one to orient these major axes in the crystal relative to the incident beam with a precision generally better than 0.1°.

A silicon surface-barrier detector with a collimating aperture 3 mm diam was used as a monitor counter in the scattering chamber. This detector was placed at a distance of 15 cm from the target, usually at about 150° to the incident beam, in such a way as to avoid any direction of high symmetry in the target crystal. The ion beam from the tandem accelerator was collimated by a 3×3-mm aperture placed 7 m before the scattering chamber and further by a circular aperture 0.8 mm diam at a distance of 50 cm before the target crystal. Another "antiscattering" aperture 1.6 mm diam was located 25 cm before the crystal. The magnetic quadrupole lenses on the beam line (which are normally used in conjunction with the scattering chamber) were turned off during these experiments. As a result of this collimation, the ion beam incident on the target crystal had a diameter of 0.8 mm and a total angular divergence of less than 0.03°.

The data were obtained by two methods. In the first method, a photographic plate was exposed to the ions emerging from the target crystal. By this means a large amount of data on the spatial distribution of these ions could be obtained quickly. No attempt was made to determine their energy distribution from a study of the photographic plates. In most cases the plates were exposed in the scattering chamber at a distance of 32.5 cm from the target so that the over-all angular resolution was limited by the size of the beam spot and was on the order of 0.15°. This angular resolution was much poorer than that obtained with the detectors as described in the next section. Nevertheless the data obtained in this way were extremly useful in giving a general "picture" of the phenomena.

In the second method, a semiconductor detector was used at the end of a relocatable extension tube attached to one of several ports in the wall of the scattering chamber. This technique permitted the recording of quantitative data on both the energy distribution and the spatial distribution of ions emerging from the target crystal. Initially[6] this type of data was taken with a position-sensitive detector which, for each particle detected, gave both a pulse proportional to the energy and a pulse proportional to the position at which the particle entered the detector. However, the resolution and linearity of the position pulse from these detectors were found to be insufficient for more accurate work. In later experiments, therefore, an experimental arrangement based on a highly collimated scanning detector was used. All of the semiconductor-counter data to be discussed in this paper were recorded with this arrangement, which we now describe in detail.

Figure 3 is a diagram of the arrangement. Ions emerging from the target crystal were detected by a

silicon surface-barrier detector mounted in a box at the end of an extension attached to one of the ports on the scattering chamber. The detector was collimated by means of a 0.625-mm-square hole in a gold foil 0.5 mm thick located immediately in front of the detector. The assembly containing the detector and its collimating aperture could be positioned within the box by means of a screw thread which was turned by a stepping motor located just outside the box. The screw had 10 threads per inch and the stepping motor required 100 steps to complete one revolution. The detector assembly was constrained to move precisely parallel to the axis of the screw thread by means of an accurately fitting nut and a guidepost also located within the box. Thus each step of the stepping motor moved the detector 0.001 in. The entire box containing the detector system could be rotated about an axis extending radially from the center of the scattering chamber and also could be given a limited linear displacement by means of the adjustments shown in Fig. 3. An on-line computer system[19] employing an ASI-210 computer was used to remotely control the position of the detector along the axis of the screw. Pulses provided by the computer were used to step the driving motor. When the motor had moved one step, this caused an optical circuit to be completed and this in turn produced an interrupt at the computer and informed the system that the task of moving the detector by 0.001 in. had been completed. The optical circuit used here consisted of a light and a photocell in conjunction with a slotted disk with 100 slots around its perimeter and mounted on the same shaft as the screw thread which positioned the detector. In addition, two limit switches were built into the box to provide a computer interrupt in the event that the detector was accidentally driven outside its normal working range.

In a typical scan taken with this detection arrangement, the orientation of the target crystal and the orientation and position of the detector box were adjusted so that some crystallographic direction (e.g., some major axis) was directed toward the center of the detector box. A scan then usually consisted in first positioning the detector at the bottom of the box and
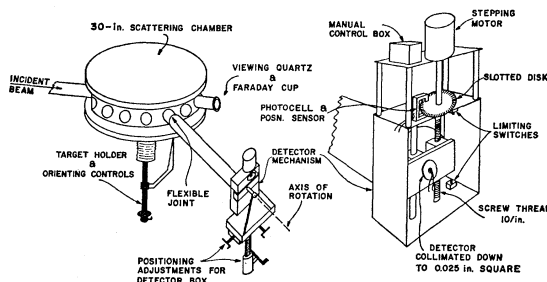

FIG. 3. Target-chamber assembly and details of the box containing the scanning semiconductor detector.

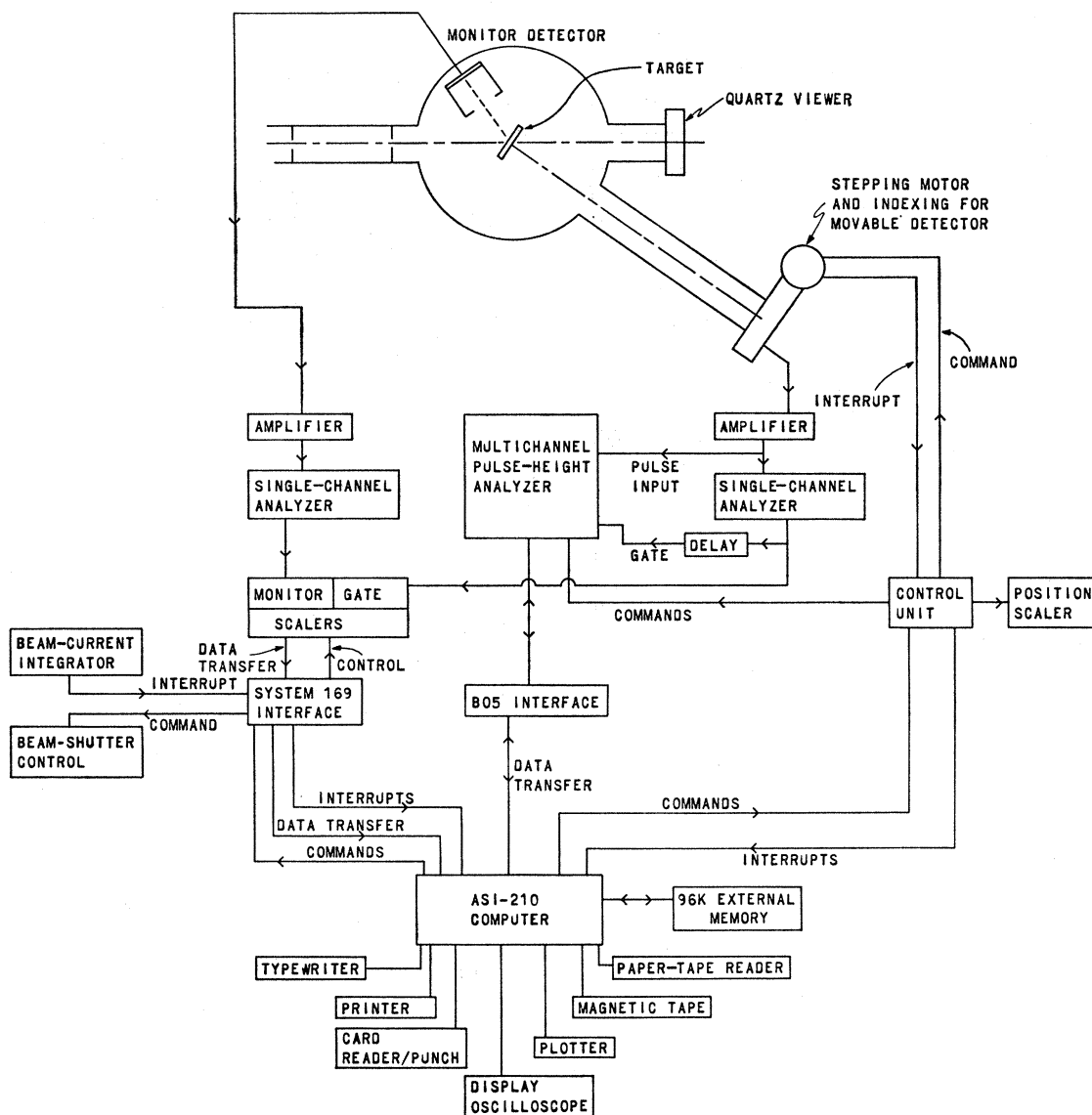[19] D. S. Gemmell, Nucl. Instr. Methods **46**, 1 (1967).

FIG. 4. Schematic diagram showing the organization of the electronics and the computer system.

then driving it under computer control over a distance of 2–3 in., typically in steps of 0.025 in. At each position along the scan, an energy spectrum of particles scattered in the target crystal was recorded for a fixed amount of integrated beam current. Figure 4 is a schematic diagram of the data-recording system. In recording the data from these experiments, the pulse-height spectra from the movable detector were recorded in an ND-160 pulse-height analyzer which is interfaced to the computer[19] in such a way that the contents of its memory could be transferred to the computer memory. In addition, the mode (i.e., analyze, stop, read-out) of the analyzer could be controlled by the computer.

The computer subroutines used for data handling and for control of the detector were called from a FORTRAN program which was organized in a manner similar to the DIDJERIDOO program.[20] By typing in a six-character mnemonic it was possible to direct the program to perform many operations—for example, to print the data on the line printer, to display it on an oscilloscope, to analyze the area of dips in the position spectra, and so on. One such subroutine was used to record the data during the detector scan. Figure 5 shows the flow chart of this subroutine. Before entering this subroutine the program requested that several constants be entered by typewriter (e.g., the distance the detector

[20] D. S. Gemmell, Argonne National Laboratory Report No. ANL-6993 (unpublished).

```
┌─────────────────────────────────┐
│ ENTER INITIAL DETECTOR POSITION,│
│ FINAL DETECTOR POSITION, AND    │
│ DISTANCE DETECTOR IS TO BE      │
│ MOVED BETWEEN RECORDING SPECTRA │
└─────────────────────────────────┘
┌─────────────────────────────────┐
│ MOVE DETECTOR TO INITIAL        │
│ POSITION                        │
└─────────────────────────────────┘
┌─────────────────────────────────┐
│ ERASE NUCLEAR-DATA-160 ANALYZER,│
│ RESET MONITOR SCALER,           │
│ RESET GATE-PULSE SCALER         │
└─────────────────────────────────┘
┌─────────────────────────────────┐
│ START NUCLEAR-DATA-160 ANALYZER,│
│ START MONITOR SCALER,           │
│ START GATE-PULSE SCALER         │
└─────────────────────────────────┘
┌─────────────────────────────────┐
│ DISPLAY DATA WHILE WAITING FOR  │
│ BEAM-CURRENT-INTEGRATOR         │
│ INTERRUPT                       │
└─────────────────────────────────┘
┌──────────────────────────┐
│ BEAM-CURRENT-INTEGRATOR  │
│ INTERRUPT                │
└──────────────────────────┘
┌─────────────────────────────────┐
│ STOP NUCLEAR-DATA-160 ANALYZER, │
│ STOP SCALERS                    │
└─────────────────────────────────┘
┌─────────────────────────────────┐
│ READ NUCLEAR-DATA-160 ANALYZER, │
│ READ SCALERS                    │
└─────────────────────────────────┘
┌─────────────────────────────────┐
│ MAKE DEAD-TIME CORRECTION AND   │
│ NORMALIZE DATA TO MONITOR       │
│ COUNT                           │
└─────────────────────────────────┘
┌─────────────────────────────────┐
│ WRITE DATA ON MAGNETIC TAPE     │
└─────────────────────────────────┘
┌─────────────────────────────────┐
│ SUM PRESELECTED REGION OF ENERGY│
│ SPECTRA AND UPDATE POSITION     │
│ SPECTRA FOR DISPLAY             │
└─────────────────────────────────┘
┌────────────────────────┐   ┌─────────────────────────────────┐
│ MOVE DETECTOR TO NEW   │   │ HAS DETECTOR POSITION EXCEEDED  │
│ POSITION AND ADJUST    │   │ LIMIT?                          │
│ POSITION SCALER        │   │      NO            YES          │
└────────────────────────┘   └─────────────────────────────────┘
                                                  ┌──────┐
                                                  │ QUIT │
                                                  └──────┘
```
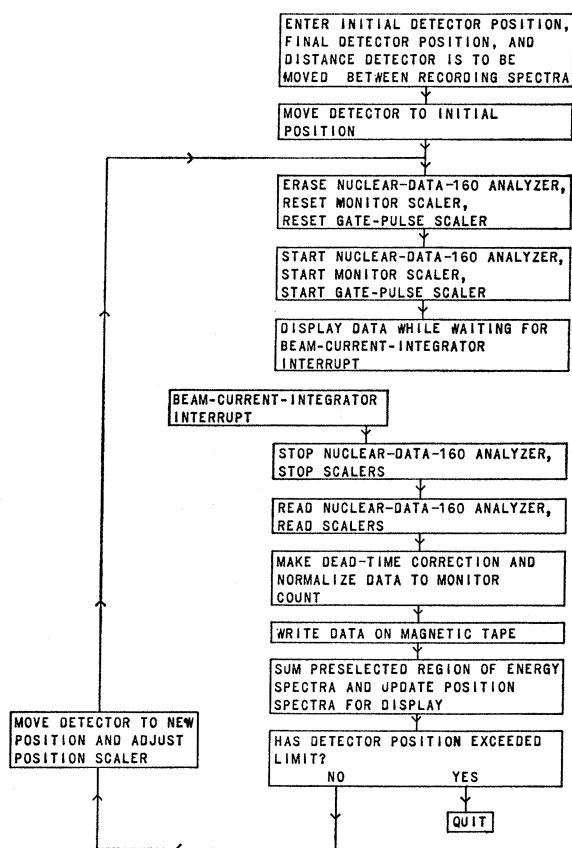
Fig. 5. Flow chart of the computer subroutine used in recording the data.

was to be moved between successive positions, the limiting position, etc.). The computer was then instructed to take a scan. After initially positioning the detector, the computer program entered the subroutine illustrated in Fig. 5. At each position in the scan, the program first erased the analyzer and reset the scaler used to count pulses from the monitor detector and also a scaler counting gate pulses applied to the pulse-height analyzer. The computer then switched the analyzer into its analyze mode and started the two scalers counting. It then displayed one of several analyses of the data already recorded on a 16-in.-diam oscilloscope while waiting for an interrupt signaling that the beam-current integrator had gone through one cycle of accumulated charge. After the detection of this interrupt, the computer stopped the pulse-height analysis and stopped the recording by the scalers. It then read the scalers and read into its memory the spectrum contained in the pulse-height analyzer. The computer then used the sum of the counts in the energy spectrum together with the reading of the scaler recording the gate pulses to perform a dead-time correction to the spectrum. It further normalized the spectrum to a fixed number of

monitor counts. This spectrum was then written onto magnetic tape and the program formed sums of counts in three preselected regions of the energy spectrum. These three sums were then used to update three "position" spectra being stored in the computer. These position spectra (counting rate as a function of position in the scan) were displayed on the oscilloscope while the next spectrum was being recorded in the pulse-height analyzer. The program supervised the movement of the detector between positions and repeated the cycle until the detector reached a predetermined limiting position.

In order to investigate an extended region, the entire box containing the detector assembly could be manually moved in both horizontal and vertical directions by use of the precision adjustments indicated in Fig. 3.

It was necessary to take great care in preparing the monocrystals to be used as targets in these experiments. It was found that unetched crystals did not produce channeling and blocking effects. Targets of silicon and germanium were produced by a diamond saw which sliced thin sections from a monocrystalline ingot. These were then cleaned ultrasonically and etched in a CP-4 etch (a solution of equal parts of concentrated nitric acid, acetic acid, and hydrochloric acid). Targets of magnesium oxide were produced by cleaving a monocrystal as described by Volpe[21] and etching with phosphoric acid. The final crystals used all had thicknesses on the order of 5–10 mg/cm² and were mounted on frames by use of a silicone rubber cement.
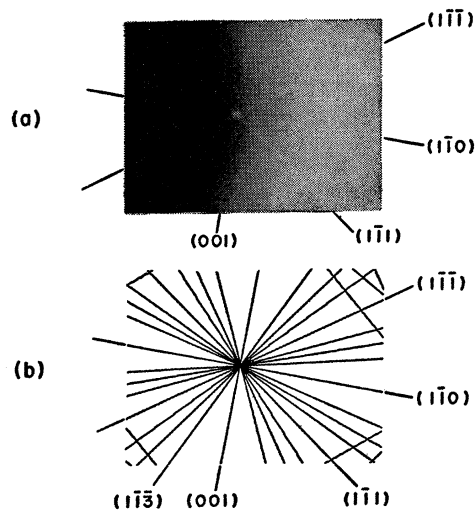

Fig. 6. Blocking pattern for a silicon crystal oriented with its [110] axis pointing at the center of the picture. (a) Experimental pattern obtained on an emulsion placed at 15° to an incident beam of 4.0-MeV protons. The angular range covered by the emulsion is about 16°. (b) Computer calculation of the lines along which the major planes of this crystal intersect the plane of the emulsion.

[21] M. L. Volpe and C. E. Paschali, Rev. Sci. Instr. **36**, 237 (1965).

$E_p = 4$ MeV
TARGET SILICON CRYSTAL (35μ)
INCIDENT BEAM "UNORIENTED"
DETECTOR AT 15° TO BEAM DIRECTION
SCANNING 0.5° AWAY FROM [110] AXIS
AND NORMAL TO (1̄10) PLANE
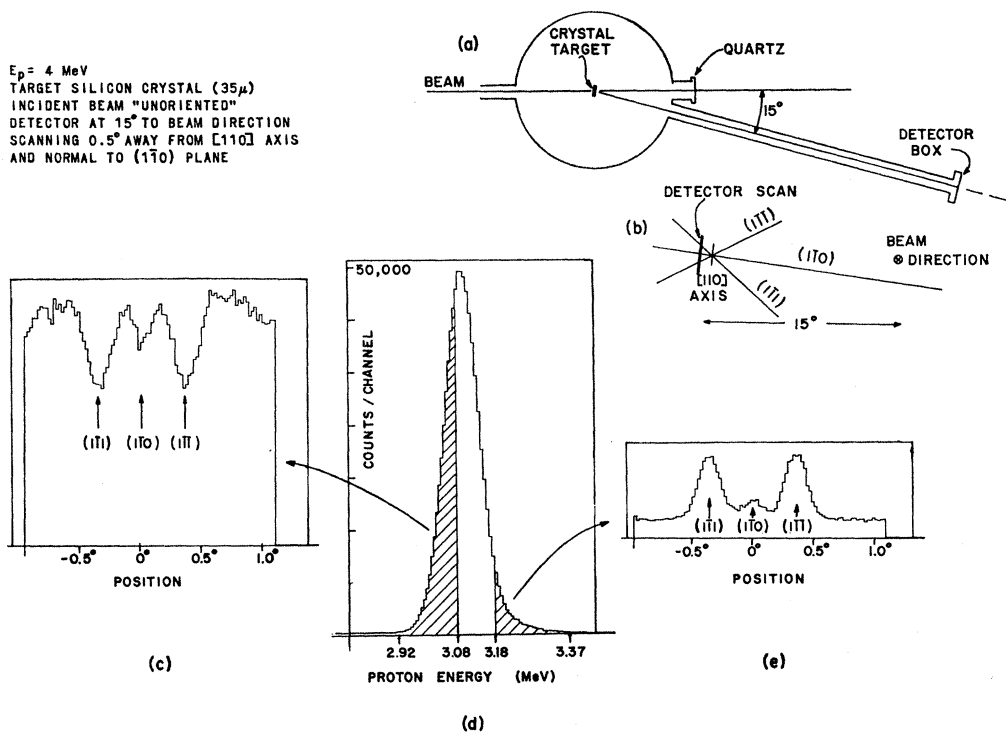
(a)

(b)

(c)

(d)

(e)

FIG. 7. "Position spectra" recorded with the scanning detector. (a) Experimental arrangement with the movable detector. (b) The path of the scan. (c) and (e) Position spectra recorded for the indicated shaded regions of energy spectrum (d). (d) Energy spectrum of the scattered protons.

3. RESULTS

A. Blocking Patterns Obtained by Photographic Technique

Figure 6 shows a typical blocking pattern observed by means of the photographic technique. The plate shown in the figure was exposed at a distance of 32.5 cm from a silicon monocrystal target oriented with its [110] axis directed toward the center of the emulsion, which was placed at 15° to the incident beam direction. The energy of the incident proton beam was 4 MeV and the thickness of the target crystal was 35 μ. The incident beam direction did not coincide with any major crystal axis or plane. The dark regions in Fig. 6 are produced where scattered protons strike the emulsion. The darkening towards the right-hand side of Fig. 6 reflects the increase in the Rutherford scattering cross section towards smaller angles. The white lines seen in Fig. 6 represent regions along which relatively few particles are detected. These "blocking" lines correspond precisely to intersections of the crystal planes with the plane of the detecting emulsion. (This was checked by means of a computer program which calculated such intersections for a specified placement of the emulsion with respect to the crystal axes. The program plotted its calculated results in a form suitable for direct comparison with the photographic emulsion. Such calcu-

lations were frequently of value in determining the identity of higher-order planes responsible for the many fainter lines observed.) The planes responsible for the lines seen in Fig. 6(a) are labeled in the accompanying diagram, Fig. 6(b). A careful study of emulsions exposed in this way has revealed faint lines corresponding to planes with Miller indices as high as 9. The white spot seen in the center of Fig. 6(a) corresponds to the point at which the [110] axis intersects the plane of the emulsion. It is interesting to note that this white spot is surrounded by an annular darker region. As one proceeds further away from the direction of the axis in Fig. 6(a), one then sees the lines arising from planar blocking.

B. Blocking Patterns Taken with Particle Detector

In order to investigate the phenomena shown in Fig. 6 in more detail, we have taken data with the scanning detector arrangement as described in the previous section. Figure 7 shows the manner in which the data were taken, together with some of the results. In the upper right-hand corner [Fig. 7(a)] is a schematic drawing of the target chamber and the detector. Below this [Fig. 7(b)] is a drawing showing the beam direction, the projected planes of the crystal, and the position at which the detector scanned the pattern. This pattern is the same as that shown in Fig. 6(b). [Figure 6(a)

INCIDENT BEAM "UNORIENTED"
DETECTOR AT 15° TO BEAM DIRECTION
SCANNING (110) PLANE
$E_p = 4.0$ MeV
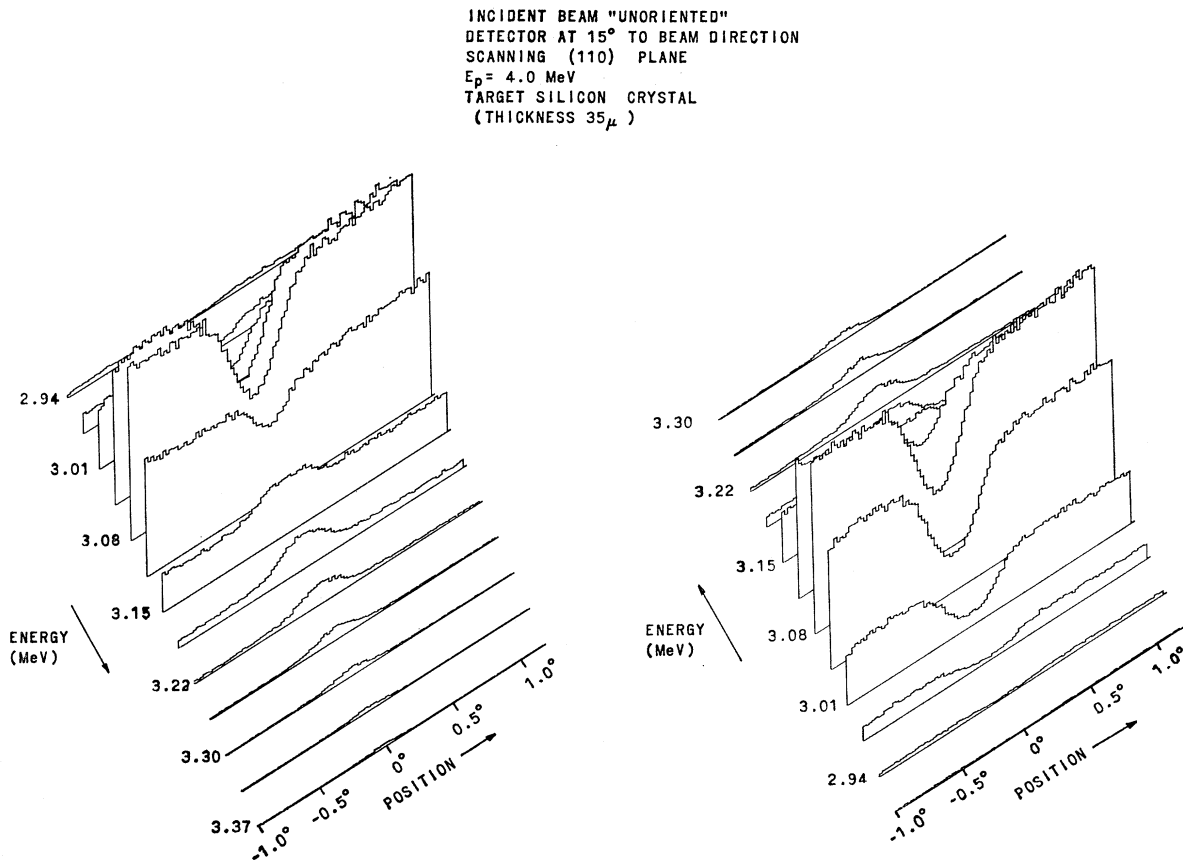TARGET SILICON CRYSTAL
(THICKNESS 35μ)

FIG. 8. Two views of a three-dimensional plot of counting rate as a function of detector position and of particle energy for a scan over the (110) plane of a 35-μ-thick silicon crystal. The incident 4.0-MeV proton beam was not directed along any major crystallographic axis of the target crystal.

was actually made by exposing an emulsion under identical conditions at 15° to the beam and just inside the main body of the target chamber.]

A typical pulse-height spectrum of protons scattered by the target crystal for one position of the scanning detector is shown in Fig. 7(d). The counts corresponding to the shaded areas in Fig. 7(d) were summed at each position of the detector. These sums are plotted in Figs. 7(c) and 7(e) as a function of the detector position during one scan which crossed the three planes indicated in Fig. 7(b). The position scale in Figs. 7(c) and 7(e) is marked in terms of angular position relative to the (110) plane. The effects of the three major planes crossed are seen clearly in the position spectra corresponding to both the low-energy and the high-energy portions of the spectrum. Whereas the low-energy part of the spectrum shows dips (blocking) corresponding to these planes, the high-energy portion shows peaks at these positions. If one integrates the position spectra over all detected proton energies, the net result shows dips at these positions—in agreement with the photographic data shown in Fig. 6(a).

In Fig. 8, we show the result of a scan across the (110) plane in a fashion similar to that illustrated in Fig. 7, except that now the detector is scanning a region further away from the [110] axis so that only one plane [the (110)] is observed. Figure 8 shows two views of a three-dimensional plot of the counting rate in the detector as a function of the energy of the detected particle and of the detector position during the scan. Here one clearly sees the transition from a dip observed for low-energy detected particles to a peak observed for the high-energy tail of the particle spectrum. The angular width of the dips is the same as that of the peaks in both cases.

Figure 9 shows the result of a sequence of scans covering a 2.0°×2.5° angular region in the neighborhood of the [110] axis. The data plotted in Fig. 9 are the counting rates [i.e., sums taken over the shaded regions of pulse height defined in Fig. 7(d)] as a function of detector position in two dimensions. The data for low-energy particles are given in Fig. 9(a). For the higher-energy particles [Fig. 9(b)], the intensity of the peak relative to off-plane background continues to increase
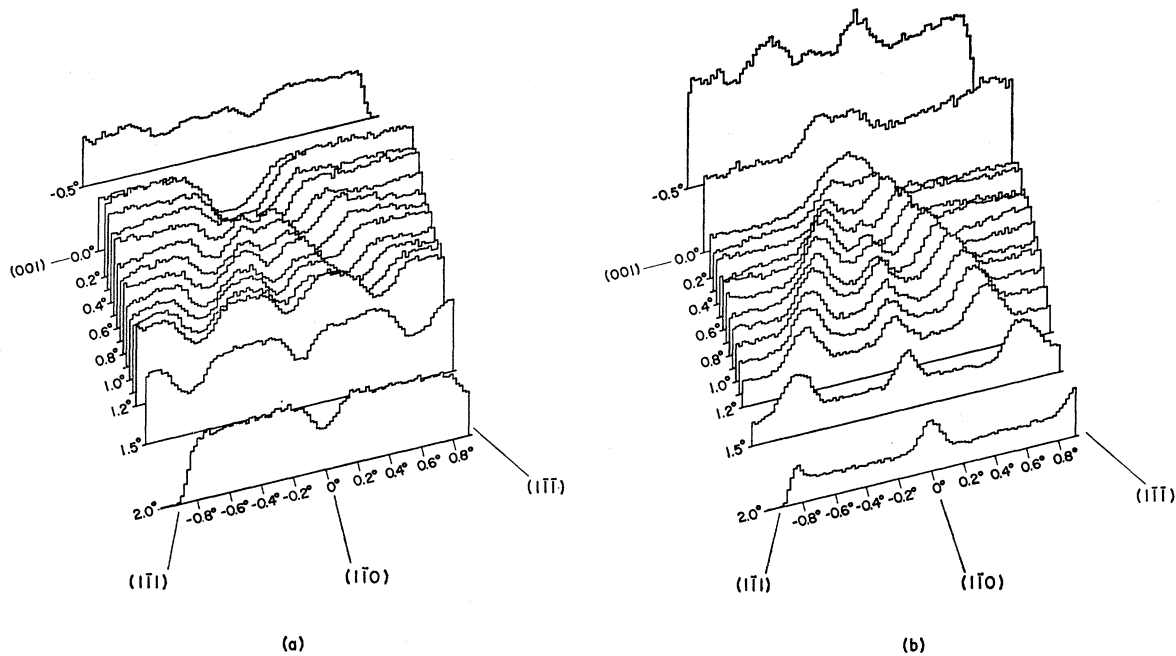
(a)

(b)

FIG. 9. Data obtained by scanning an extended region of space (2.0°×2.5° in angular dimensions) near the [110] axis in an arrangement as shown in Fig. 7. (a) The distribution of low-energy particles. (b) The distribution of high-energy particles.

as one approaches the beam direction. This would indicate that these high-energy particles are particles that are initially channeled and, as a result of a series of small-angle scatterings while in the planar channel, are deflected to the detector. Some additional data concerning these particles with abnormally low energy losses are given in Sec. 3 H. In Fig. 9(a), the dip associated with the [110] axis corresponds to a 90% reduction in the intensity of detected particles. For both high- and low-energy particles, one also observes anomalous behavior in the near vicinity of the axis — just as in the photographic data of Fig. 6(a). That is, the intensity of the dip [Fig. 9(a)] or peak [Fig. 9(b)] becomes much weaker nearer the axis.

C. Calculation of Particle Trajectories in a Model Lattice

A very much simplified model of the crystal and of the interaction with positive ions was assumed in a computer calculation to see whether some of the effects seen in the blocking experiments could be reproduced by calculations. For the purposes of the calculation we adopted a model of the crystal lattice in which the nuclei of the crystal atoms are considered to be rigidly fixed massive point charges distributed throughout a regular rectangular lattice. Thus we ignored thermal vibrations and recoil effects during the scattering process. Our model crystal was further assumed to contain no electrons. Thus the basic interaction between ion and lattice was taken to be a pure unscreened Coulomb potential and we disregarded the slowing-down effect of the electrons that would normally be present.

{Note added in proof: In a recent paper, J. V. Anderson [Kgl. Danske Videnskab. Selskab, Mat.-Fys. Medd. 36, No. 7 (1967)] has calculated the shape of the dip expected from blocking. His treatment uses a shielded potential and thermal vibration is partially taken into account by assuming that the emitting nucleus vibrates (the rest of the lattice is taken as stationary). In contrast to our treatment which follows the particle through the lattice and treats each scattering event individually, he has used the continuum approximation of Lindhard.}

The computer program (a FORTRAN program written for the ASI 2100) calculated trajectories for ions emitted isotropically from a lattice site. Initial angles of emission for the particles were chosen by use of random numbers generated by the computer Only particles initially emitted within 3° of the [100] axis were considered. As an ion passed through successive layers of the lattice, the effect of Rutherford scattering from the nearest lattice point in each layer was calculated and a new set of direction cosines was produced. Each path was followed until the ion had passed through a predetermined thickness of the lattice. The exit angle of each path relative to the [100] axis was recorded on a punched card. These exit angles are plotted in Fig. 10 for a number of different thicknesses of the lattice. The parameters used in Eq. (1) to calculate the points
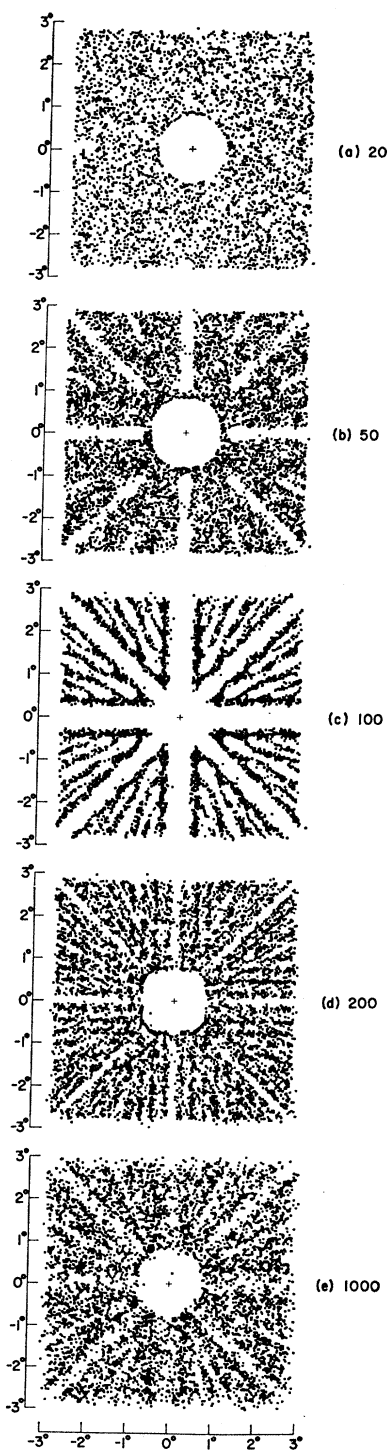
FIG. 10. Plots of the calculated distributions of particles emerging from a hypothetical lattice as determined by the "computer experiment" described in the text. The successive plots are made for ions that have passed through lattices 20, 50, 100, 200, and 1000 atoms thick. The central "hole" in the distribution is simply that expected from the Coulomb shadow effect in the direction of the [100] axis.

shown in Fig. 10 were $Z_1 = 1$, $Z_2 = 14$, $l = 2.5$ Å, $E = 4.0$ MeV. For small lattice thicknesses, the calculated pattern is strongly affected by the limited number of layers traversed. As more layers are traversed, some semblance of a blocking pattern begins to develop and after passing through 1000 atomic layers, this pattern has more or less stabilized. One can clearly see blocking at the [100] axis and also at the (101), (001), (011), and (012) planes, as well as for higher-order planes.

A comparison of the widths of lines found in this calculation with other theoretical estimates of the widths and measurements of the widths is given in Sec. 3D. One should also notice that these calculations predict a behavior in the vicinity of an axis similar to that observed; that is, the dip arising from blocking in a plane becomes much weaker near an axis.

D. Width of Blocking Patterns and Its Energy Independence

In this section, we discuss our measurements of the widths of the blocking lines, compare them with theoretical estimates, and relate them to other measurements in somewhat different experiments. In comparing measurements, it is convenient to distinguish between the width of a blocking pattern for planar blocking (a line) and for axial blocking (a spot). Although for silicon these observed widths are very nearly the same, in tungsten a spot is roughly three times as wide as a line. Our experimental arrangement made it difficult to accurately measure the width for axial blocking since a slight error in locating the position of an axis could lead to a measurement that overestimates the width. Because of this we give only an upper limit for the width in axial blocking. Our measurements are for planar blocking in silicon; the measurements by Domeij[17] and by Tulinov[15] are for axial blocking in tungsten, and are not directly comparable.

The widths associated with planar blocking were measured by observing the number of scattered particles as a function of emergence angle along a line perpendicular to the (110) plane of a silicon crystal (11 mg/cm² thick) with the incident protons at energies between 3 and 12 MeV. The incident beam entered about 3° from the [122] axis and was not on a low-index planar or axial channel. The emerging protons were detected at an angle of 15° with respect to the incident beam and were not near a low-index axis. In Fig. 11, the number of particles in the high-energy-loss part of the pulse-height spectrum of the emerging protons has been plotted as a function of the angle measured from the (110) plane for three of the energies used. Figure 12 is a plot of the full width at half-maximum as a function of the average energy of protons traversing the crystal. The variation of width with energy is well represented by $E^{-1/2}$. The magnitude of the width is about a sixth of the value β given by Eq. (1), and about a half of Lindhard's estimate for planar blocking. The calcu-

lations of Sec. 3 C, which are based on a rigid lattice, give a width for planar blocking about twice that observed.

The widths of blocking lines have also been studied by Domeij[17] for α particles from Rn^{222} embedded in tungsten crystals and by Tulinov et al.,[15] who used protons reflected by tungsten crystals. Domeij found widths of approximately 0.5° for planar blocking and of 1.6° for axial blocking for 6.0-MeV α particles. These values are somewhat smaller than Lindhard's prediction. The measurements of Tulinov et al. on elastically scattered protons of 3 MeV from tungsten are in agreement with the results of Domeij. Tulinov's measured width of the dip for axial blocking in tungsten was consistent with that measured by Domeij. Tulinov presented no quantitative data for planar blocking, but from inspection of the reproductions of emulsions exposed to 200-keV protons scattered from tungsten one concludes that the width for planar blocking is again only about a third of the width for axial blocking.

Table I lists these experimental results as well as the results of the calculation described in Sec. 3 C and the observations of the other experiments on blocking. The first (left-hand) section of Table I lists the various experimental conditions. The second and third sections give the observed and calculated full widths for axial and planar blocking. The theoretical estimates shown are for a static lattice and were derived as the limiting angles relative to an axis or plane for channeled particles: but since a particle is removed from a channel by
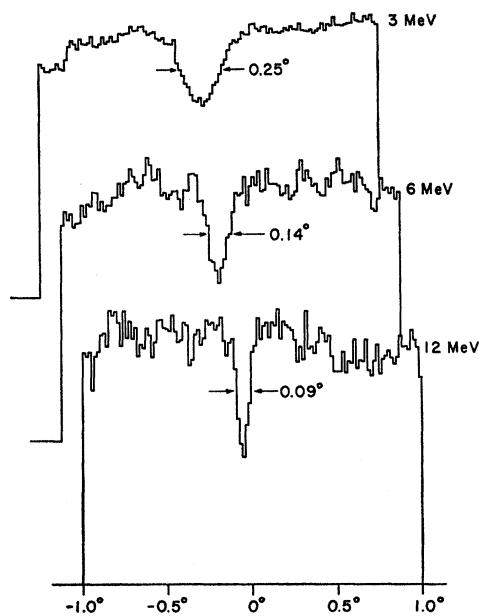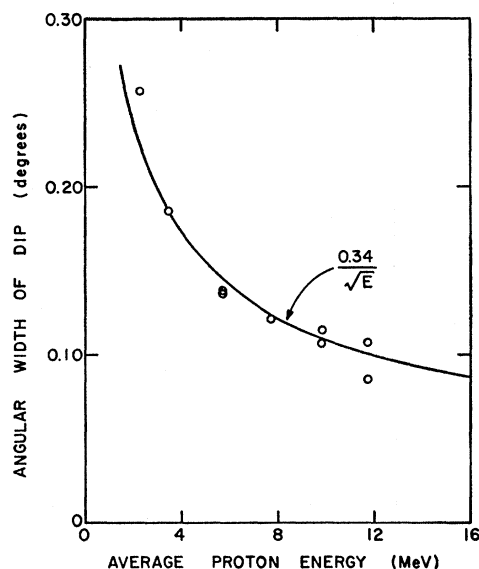

FIG. 12. Plot of the total angular widths of dips (such as those shown in Fig. 11) as a function of the average beam energy in the target crystal. The data points have been fitted with an inverse-square-root curve.

collision with a lattice site, and the time-reversed path (neglecting energy loss) corresponds to one for which a particle is emitted from a lattice site, we expect that such estimates for channeling will also apply to blocking. This reciprocity was recently demonstrated by Bøgh and Whitton[22] with 1-MeV protons on tungsten. Lindhard's estimate[2] of the width for axial scattering is $2C(2Z_1Z_2e^2/lE)^{1/2}$; and this is equal to the value of β given by Eq. (1) if we take $C=\sqrt{2}$ as Domeij does. Lindhard's estimate for planar blocking is

$$\frac{2C(2Z_1Z_2e^2/\bar{d}E)^{1/2}}{2Z_2^{1/6}},$$

where $\bar{d}$ is the mean lattice spacing in the plane (i.e., $1/\sqrt{n}$, where n is the atomic density in the plane). This is an approximate expression for low-index planes. Erginsoy[3] has made similar calculations for a variety of approximations to the Thomas-Fermi potential both for rows of atoms and for planes, and in the latter case has explicit kept the dependence on density in the plane. All of these estimates are based on the idea that a row or plane may be replaced by an average potential so that the energy of motion transverse to the row or plane is conserved. Under these assumptions, the maximum angle the path of the particle can have relative to a row or plane is simply related to the potential energy at the point of closest approach to the row or plane. Both Lindhard and Erginsoy take this point of closest approach as the screening radius of the potential.

In Table I, the entries in the columns labeled "Erginsoy" were computed by use of the Moliére

FIG. 11. Position spectra recorded at three bombarding proton energies for scans made at right angles to the (110) plane of a 35-μ-thick silicon crystal. Elastically scattered protons were detected around 15° to the incident beam direction. The plots shown are those for the low-energy (high-loss) part of the recorded energy spectra.

[22] E. Bøgh and J. L. Whitton, Phys. Rev. Letters **19**, 553 (1967).

TABLE I. Summary of observations and calculations on blocking widths. The angular widths quoted are the full widths at half-maximum.

Exptl.	Resol.	Particle	E (MeV)	Crystal	Dir.	l (Å)	Axial Obs.	Axial Lind-hard[a]	Axial Ergin-soy[b]	Dir.	d (Å)	Planar Obs.	Planar Lind-hard[a]	Planar Ergin-soy[b]
Present work	0.03°	p	4.0	Si	[110]	3.84	≤0.34°	0.83°	0.47°	(110)	3.23	0.19°	0.29°	0.21°
Computer experiment[c]	...	p	4.0	$Z_2=14$	[100]	2.5	1.71°	1.03°	1.2°	(100)	2.5	0.43°	0.33°	...
Domeij[d]	0.3°	α	6.0	W	[111]	2.74	1.6°	2.61°	1.49°	(110)	2.66	0.45°	0.65°	0.63°
Tulinov et al.[e]	0.5°	p	3.0	W	[111]	2.74	~2°	2.61°	1.49°					

a Reference 2, with $C=\sqrt{3}$. For the axial case, the results are identical with Eq. (1).

b Reference 3. The potentials used are the Molière approximation to the static Thomas-Fermi potential, except for the "computer experiment," where our unscreened static Coulomb potential was taken for the axial case. (For the planar case, the approximation of an unscreened sheet potential was considered inappropriate since there would be zero electric field everywhere within a planar channel.) The potentials were evaluated at $\rho = a_{TF}$ (the Thomas-Fermi screening distance). For the axial case, the potential taken is that of a single atomic row. For the planar case, the potential was made to be zero in the middle of the planar channel.

c See Sec. 3 C.

d Reference 17. Measurements were made for $E_\alpha = 5.5$, 6.0, and 7.7 MeV.

e Reference 15.

potential, except that the entry in the row labeled "Computer experiment" was calculated with the unscreened Coulomb potential. The estimates shown in Table I are usually within a factor of 2 of the observed full width at half-maximum.

E. Transition from Blocking to Channeling

Channeling effects are seen when the incident beam is directed almost parallel to a major crystal plane. An example of a channeling pattern is seen in Fig. 13(a), which shows the result of exposing an emulsion to a 4-MeV proton beam transmitted through a germanium crystal (5 mg/cm² thick) oriented with its [111] axis in the beam direction. Within the region of multiple scattering (approximately ±2° to the beam direction), one sees the characteristic star pattern corresponding to a concentration of particles channeled into the associated (110) planes. One also sees fainter lines corresponding to channeling in higher-order planes. At angles farther from the beam direction (i.e., entering the region in which the dominant process becomes a single wide-angle scattering in the crystal), one sees the transition to a blocking effect [i.e., an absence of particles in the direction of the (110) and higher-order planes]. Again the widths of the blocking and channeling lines appear to be about equal—although the size of the beam spot limits the angular resolution in these emulsion measurements.

Figure 13(b) shows the result of exposing an emulsion under the same conditions as for Fig. 13(a), except that the target crystal has now been tilted upwards by about
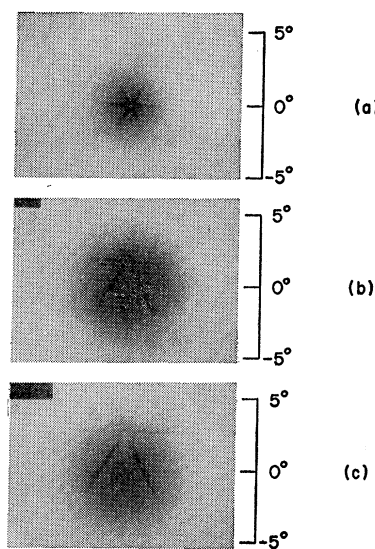

FIG. 13. "Star" patterns obtained by exposing photographic plates to a 4-MeV proton beam transmitted through a thin (5 mg/cm²) germanium crystal oriented with its [111] axis close to the beam direction. The angle between beam and [111] axis is close to 0° in (a), ~0.2° in (b), and ~2° in (c). The dark lines correspond to intensifications due to channeling and the white lines are extinctions due to blocking in the associated planes.

0.2°. As a consequence, the associated blocking and channeling patterns have moved correspondingly, and the star pattern due to channeling is now spread over a larger angular region. Figure 13(c) shows the result of tilting the crystal approximately 2° upwards. The [111] axis now produces a net extinction at its point of intersection with the emulsion.

F. Structure Within the Lines

Figure 14(a) shows a pattern obtained with a crystal oriented so that a major plane [here the (110) plane] runs through the edge of the region of multiple scattering. In cases such as this, the corresponding line in the emulsion is observed to contain structure. The line becomes darker (more particles) on the side away from the beam direction and lighter (fewer particles) on the side nearest the beam direction. Figure 14(b) is a schematic representation of the observed effect. The blocking line actually bends inward toward the beam direction as it passes through the edge of the multiple-scattering region.

It is of interest to point out the similarity to the well-known Kikuchi patterns[23] observed in electron diffraction with thick monocrystalline samples. Kikuchi patterns arise as a consequence of multiple scattering in the sample. This multiple scattering results in a roughly Gaussian spreading of directions of the electrons in the incident beam. For a given plane, therefore, more electrons diffract from the nearer side than from the farther side of the beam direction. The resulting diffraction pattern on a photographic plate has a dark line away from the beam and a light line closer to the beam. These two parallel lines are equidistant from the projection of the diffracting plane onto the emulsion. Kikuchi patterns have been observed[24] at incident
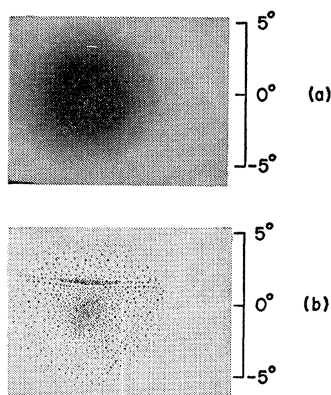
FIG. 14. Pattern produced by a beam of 4-MeV protons transmitted through a 35-μ-thick silicon crystal oriented so that the (110) plane traverses the edge of the region of multiple scattering: (a) as obtained on a photographic emulsion, and (b) as a schematic diagram.

[23] S. Kikuchi, J. Phys. Soc. Japan **5**, 83 (1928).
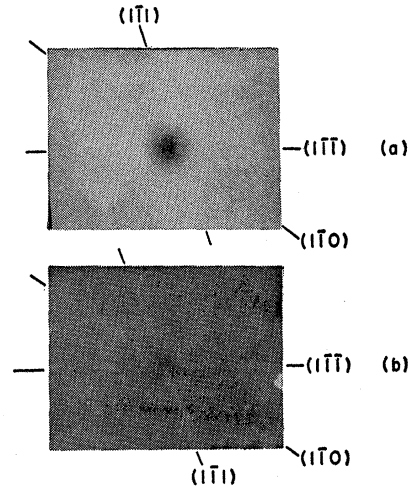[24] G. DuPouy and F. Perrier, J. Microscopie **3**, 233 (1964).

FIG. 15. Comparison between the "star" patterns produced on photographic plates (a) by channeling of 6-MeV deuterons and (b) by blocking of protons from the Si^{28} (d, p) reaction. The silicon crystal used for both cases was 35 μ thick and was oriented with its [110] axis in the beam direction; the only difference between the two experimental arrangements was that in (b) the deuterons were stopped by a gold foil covering the emulsion.

electron energies up to 1 MeV ($\lambda = 0.008$ Å). Since our experiment shows a somewhat similar pattern in the region of multiple-scattering protons, it is tempting to attribute the effect to diffraction.[25] Fowler and Erginsoy[26] and DeWames et al.[27] have commented on this question of wave phenomena in crystals. Other discussions of this phenomena have been given by Appleton et al., by N. W. Thompson, and by Dearnaley et al. at a recent meeting.[28]

G. Effects Seen with (d, p) Reaction

The observation of protons emitted from the (d, p) reaction on nuclei in a monocrystal affords an opportunity to isolate effects associated with the emission of ions directly from the crystal nuclei from effects associated with the incident beam.

A beam of 6-MeV deuterons was directed into the scattering chamber (Fig. 2) and was incident upon a silicon crystal (10 mg/cm² thick) oriented with its [110] axis in the beam direction. Two photographic plates were exposed successively at 0° to the beam direction. The first was briefly exposed to the deuteron beam directly transmitted through the crystal. The result [Fig. 15(a)] shows a channeling pattern at small angles going over to a blocking pattern outside the region of multiple scattering (similar to the patterns seen in

[25] R. E. DeWames, W. F. Hall, and G. W. Lehman, Phys. Rev. **148**, 181 (1966).
[26] H. A. Fowler and C. Erginsoy, Phys. Letters **24A**, 390 (1967).
[27] R. E. DeWames, W. F. Hall, and L. T. Chadderton, Phys. Letters **24A**, 686 (1967).
[28] Brookhaven National Laboratory Report No. BNL-50083 (C-52), edited by A. N. Goland (unpublished). See particularly papers by B. R. Appleton, L. C. Feldman, and W. L. Brown, by N. W. Thompson, and by Dearnaley et al.
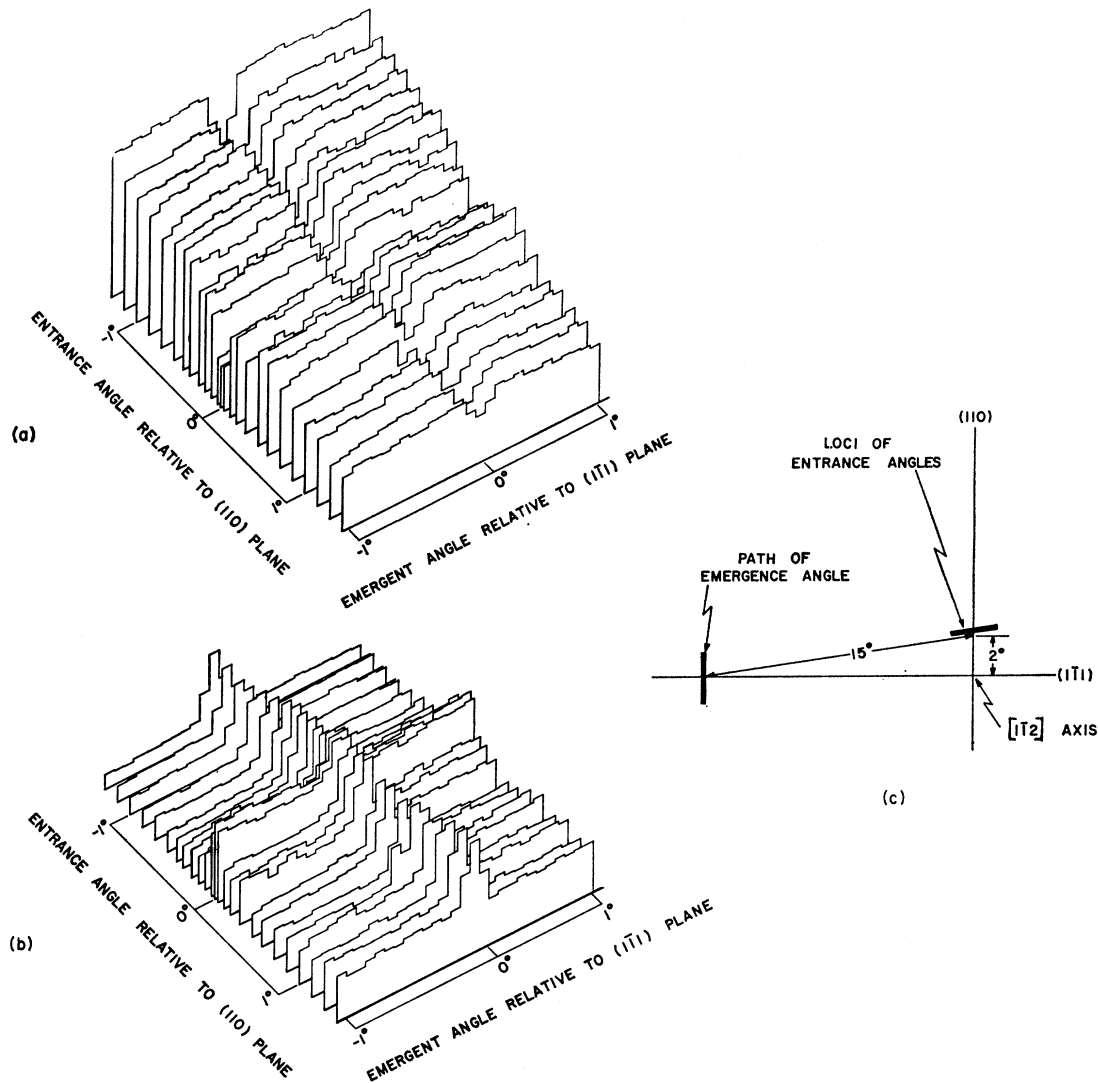
FIG. 16. Data on the variation in the number of scattered particles as a function of incident beam direction and emergence angle. (a) Number of scattered particles with more than normal energy loss. (b) Number of scattered particles with less than normal energy loss. (c) Gnomonic projection of crystal planes and the range of entrance and emergence angles used in obtaining the data in (a) and (b).

exposures to proton and α-particle beams). The second emulsion was exposed for a much longer time in the same position but now covered with a gold foil (0.003 in. thick). This foil was thick enough to stop the transmitted deuteron beam but not to stop protons from the $Si^{28}(d, p)Si^{29}$ reaction ($Q=+6.2$ MeV) whose energies range up to 12.2 MeV. The result [Fig. 15(b)] shows a pure blocking pattern even at 0° to the beam direction. [The ($l=0$) angular distribution of protons leading to the ground state of Si^{29} is strongly peaked around 0°.]

The difference between these two exposures is a further indication that the blocking effect is a consequence of particle trajectories originating at the nuclei of a crystal.

H. Dependence of Blocking Effects on Orientation Relative to the Incident Beam

Since Rutherford scattering is an example of a reaction that requires rather close collisions in order to produce large-angle scattering, we should expect changes in the number and spectrum of scattered particles when the incident beam is near a channeling direction. This section is a discussion of data taken to explore these effects when the incident beam enters along a planar channel.

A silicon target crystal 35 μ thick was oriented as shown in Fig. 16(c). In this gnomonic projection of the crystal planes and axes, the incident beam direction can

be represented by a point; distances between points on the diagram represent angles between the corresponding directions. In this experiment we require the incident beam direction to correspond to a point on the line marked "locus of entrance angles." After an entrance angle had been chosen, a scan of the emergent particles was taken along the line marked "path of emergence angles" with the detector arrangement shown in Fig. 3 and described in Sec. 2. This procedure was repeated with the entrance angle changed by 0.15° (or less in the vicinity of the plane) until the data had been obtained for a sequence of points along the line marked "locus of entrance angles."

The results of these scans are shown in Figs. 16(a) and 16(b). The measurements were made with an incident beam of 4-MeV protons. Figure 16(a) shows the series of position spectra obtained for the normal-energy-loss component and Fig. 16(b) that for the low-energy-loss component of the detected protons. It will be observed from Fig. 16 that when the incident beam is "unoriented"—i.e., removed from the (110) or any other major plane—data similar to those of Figs. 7 and 8 are obtained. However, when the incident beam lies in the (110) plane, one notices two important effects: (1) the normal-energy-loss component is sharply reduced in intensity and (2) the low-energy-loss component detected off the (111) plane is sharply increased in intensity, while that detected on the (111) plane is affected little if at all. The first of these two effects may be interpreted simply as being due to the reduced nuclear reaction rate when the incident beam is channeled. The scattered fraction of the beam (and we have here selected the component that undergoes a single large-angle scattering) shows the usual blocking effect at the (111) plane.

The second effect would appear to have a more complicated origin. When both the incident beam and the direction in which the detected particles emerge are "unoriented," the fraction of detected particles having a low energy loss is very small. When the emergent particles are detected in the direction of a major plane, one observes a sharp increase in the number of low-energy-loss particles detected. Presumably these particles reach the detector by the normal process of multiple scattering and the enhancement of their intensity is caused by their becoming trapped in the planar channel—in this case, the (111). When, in addition, the incident beam is channeled, one can suppose that two opposing effects come into play. The reaction rate between the incident beam and the nuclei in the target crystal is reduced. On the other hand, those particles that do scatter out of the incident beam will tend to have low energy losses because of the abnormally low energy loss for the channeled beam. These opposing tendencies may account for the insensitivity to the incident beam orientation of the low-loss particles detected in the (111) plane [Fig. 16(b)]. When the emergent particles are detected in a direction away from a major plane [the (111) in this case] but the incident beam is channeled [in the (110) plane here], one might expect an increase of low-loss particles (as compared with the case of an "unoriented" incident beam) simply because of the low energy loss in the channeled beam.

Measurements of the type described in this section afford a new means of determining channeling widths. The total angular widths of the dips [Fig. 16(a)] and peaks [Fig. 16(b)] caused by channeling of the incident beam were determined at 0.18°. Thus the angular half-width is 0.09°, a value consistent with the determination of Gibson et al.,[10] who observed that for 5-MeV protons the half-angle is less than 0.1°. For 5-MeV protons, Erginsoy[3] calculates that the angular half-width for channeling is 0.09° for the (110) plane.
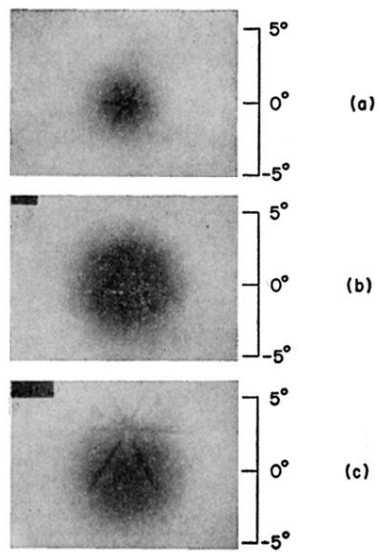
ACKNOWLEDGMENTS

FIG. 13. "Star" patterns obtained by exposing photographic plates to a 4-MeV proton beam transmitted through a thin (5 mg/cm²) germanium crystal oriented with its [111] axis close to the beam direction. The angle between beam and [111] axis is close to 0° in (a), ~0.2° in (b), and ~2° in (c). The dark lines correspond to intensifications due to channeling and the white lines are extinctions due to blocking in the associated planes.
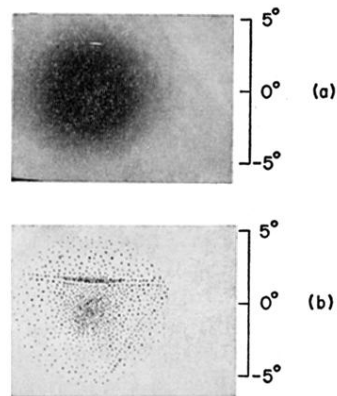
FIG. 14. Pattern produced by a beam of 4-MeV protons transmitted through a 35-μ-thick silicon crystal oriented so that the (110) plane traverses the edge of the region of multiple scattering: (a) as obtained on a photographic emulsion, and (b) as a schematic diagram.
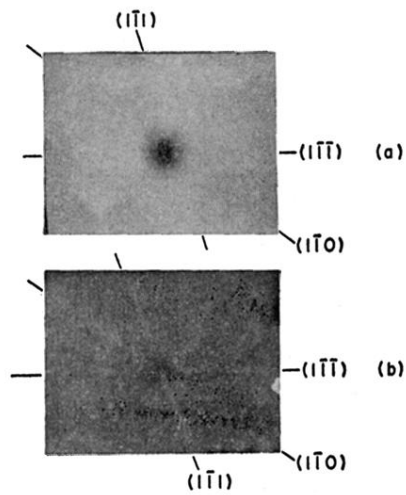
FIG. 15. Comparison between the "star" patterns produced on photographic plates (a) by channeling of 6-MeV deuterons and (b) by blocking of protons from the Si²⁸ (d, p) reaction. The silicon crystal used for both cases was 35 μ thick and was oriented with its [110] axis in the beam direction; the only difference between the two experimental arrangements was that in (b) the deuterons were stopped by a gold foil covering the emulsion.
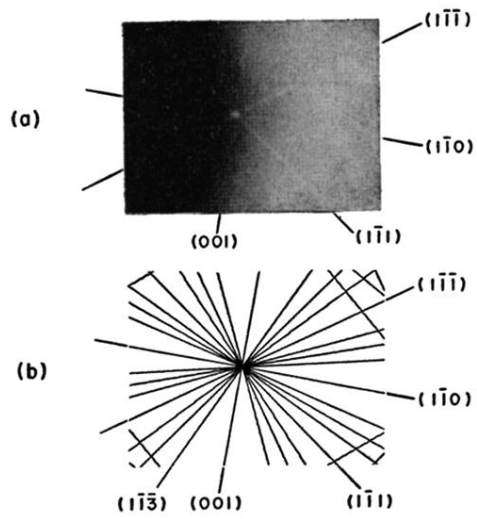
FIG. 6. Blocking pattern for a silicon crystal oriented with its [110] axis pointing at the center of the picture. (a) Experimental pattern obtained on an emulsion placed at 15° to an incident beam of 4.0-MeV protons. The angular range covered by the emulsion is about 16°. (b) Computer calculation of the lines along which the major planes of this crystal intersect the plane of the emulsion.